Chapter 5

Wetland Monitoring and Mapping Using Synthetic Aperture Radar

Mohammed Dabboor and Brian Brisco

Additional information is available at the end of the chapter

http://dx.doi.org/10.5772/intechopen.80224

Abstract

Wetlands are critical for ensuring healthy aquatic systems, preventing soil erosion, and securing groundwater reservoirs. Also, they provide habitat for many animal and plant species. Thus, the continuous monitoring and mapping of wetlands is necessary for observing effects of climate change and ensuring a healthy environment. Synthetic Aperture Radar (SAR) remote sensing satellites are active remote sensing instruments essential for monitoring wetlands, given the possibility to bypass the cloud-sensitive optical instruments and obtain satellite imagery day and night. Therefore, the purpose of this chapter is to provide an overview of the basic concepts of SAR remote sensing technology and its applications for wetland monitoring and mapping. Emphasis is given to SAR systems with full and compact polarimetric SAR capabilities. Brief discussions on the latest state-of-the-art wetland applications using SAR imagery are presented. Also, we summarize the current trends in wetland monitoring and mapping using SAR imagery. This chapter provides a good introduction to interested readers with limited background in SAR technology and its possible wetland applications.

Keywords: wetlands, SAR, satellites, monitoring, mapping

1. Introduction

Wetlands are defined based on the Canadian Wetland Classification System as land that is saturated with water long enough to promote wetland or aquatic processes as indicated by poorly drained soils, hydrophytic vegetation and various kinds of biological activity which are adapted to a wet environment [1]. Wetlands are important ecological systems which play a critical role in hydrology and act as water reservoirs, affecting water quality and controlling runoff rate [2]. Also, they are amongst the most productive ecosystems, providing food,

construction materials, transport, and coastline protection. They provide many important environmental functions and habitat for a diversity of plant and animal species [2]. Furthermore, wetlands bring economic value with social benefits for people, providing significant tourism opportunities and recreation that can be a key source of income. For these reasons, the continuous and accurate monitoring of wetlands is necessary, especially for better urban planning and improved natural resources management [3]. The formation of wetlands requires the presence of the appropriate hydrological, geomorphological and biological conditions [2].

The Canadian Wetland Classification System divides wetlands into five classes based on their developmental characteristics and the environment in which they exist [1]. As shown in **Figure 1**, these classes are: bogs, fens, marches, swamps, and shallow water. Bogs (**Figure 2a**) are peatlands with a peat layer of at least 40 cm thickness, consisting partially decomposed plants. Bogs surface is usually higher relatively to the surrounding landscape and characterized by evergreen trees and shrubs and covered by sphagnum moss. The only source of water and nutrients in this type of wetlands is the rainfall [4]. Bogs are extremely low in mineral nutrients and tend to be strongly acidic [1].

Like bogs, fens (**Figure 2b**) are also peatlands that accumulate peats. Fens occurs in regions where the ground water discharges to the surface [1]. This type of wetlands is usually covered by grasses, sedges, reeds, and wildflowers. Typically, fens have more nutrients than bogs, and the water is less acidic [4]. Marshes (**Figure 2c**) are wetlands that are periodically or permanently flooded with standing or slowly moving water and hence are rich in nutrients [4]. Some marshes accumulate peats, though many do not. Marshes are characterized by non-woody vegetation, such as cattails, rushes, reeds, grasses and sedges [1]. Similar to marshes, swamps (**Figure 2d**) are wetlands that are subject to relatively large seasonal water level fluctuations [4]. Swamps are characterized by woody vegetation, such as dense coniferous or deciduous forest and tall shrubs. Some marshes accumulate peats, though many do not [1]. Shallow open water wetlands (**Figure 2e**) are ponds of standing water bodies, which represent a transition

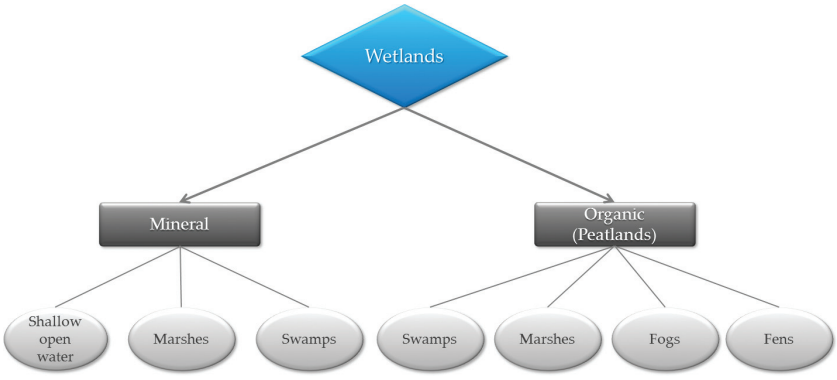

Figure 1. Wetland classes hierarchy.

http://dx.doi.org/10.5772/intechopen.80224

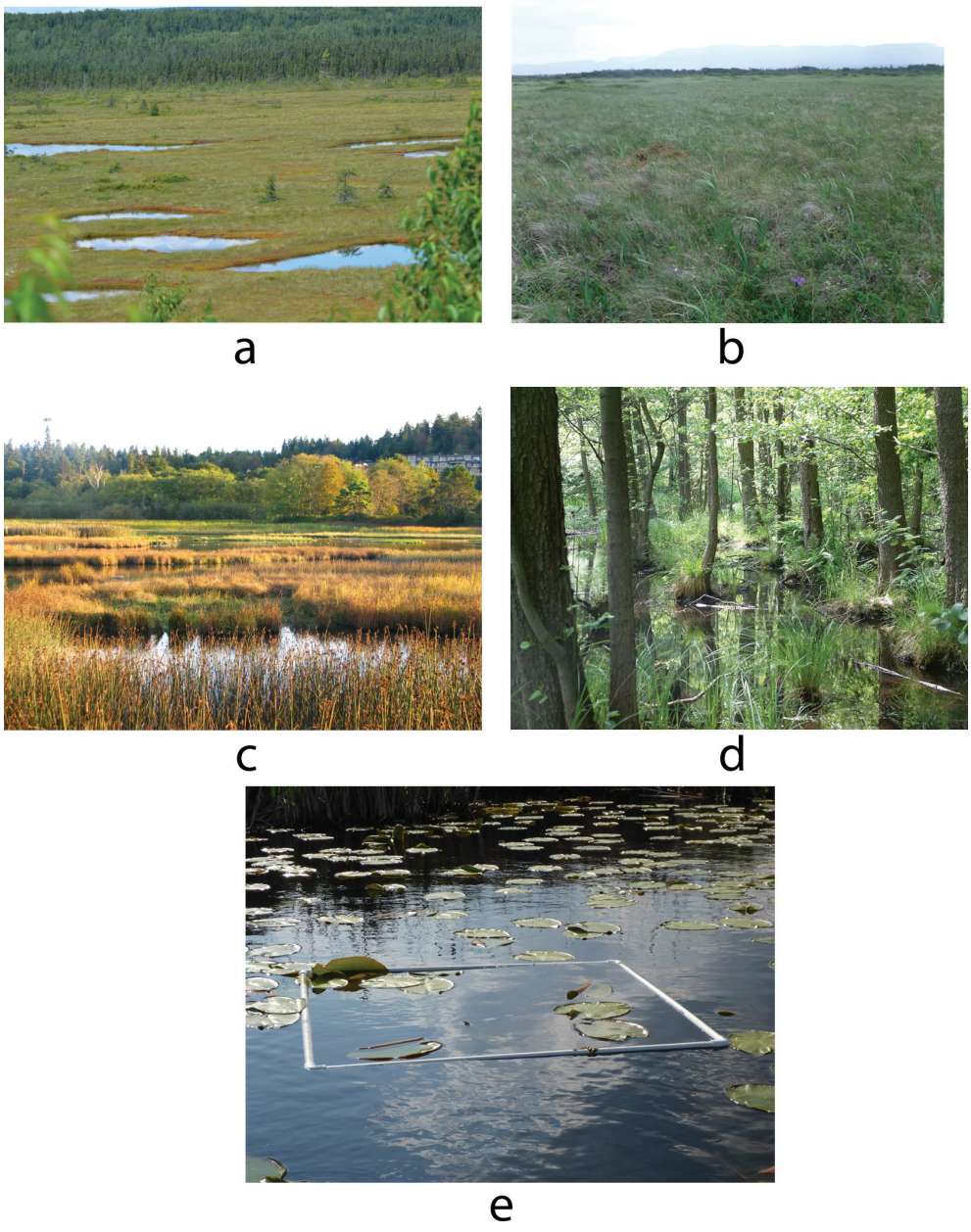

Figure 2. Wetland classes as defined by the Canadian Wetland Classification System: (a) bog, (b) fen, (c) marsh, (d) swamp and (e) shallow open water.

stage between lakes and marshes. This type of wetlands is free of vegetation with a depth of less than 2 m [1].

Spaceborne remote sensing technology is necessary for effective monitoring and mapping of wetlands. The use of this technology provides a practical monitoring and mapping approach of wetlands, especially for those located in remote areas [5].

2. Basic SAR concepts

Wetlands are usually located in remote areas with limited accessibility. Thus, remote sensing technology is attractive for mapping and monitoring wetlands. Synthetic Aperture Radar (SAR) systems are active remote sensing systems independent of weather and sun illumination. SAR systems transmit electromagnetic microwave from their radar antenna and record the backscattered signal from the radar target [6]. The sensitivity of SAR sensors is a function of the: (1) band, polarization, and incidence angle of the transmitted electromagnetic signal and (2) geometric and dielectric properties of the radar target [7]. Radar targets can be discriminated in a SAR image if their backscattering components are different and the radar spatial resolution is sufficient to distinguish between targets [6]. Conventional SAR systems are linearly polarized radar systems which transmit horizontally and/or vertically polarized radar signal and receive the horizontal and/or vertical polarized components of the backscattered signal (**Figure 3**). In SAR systems, polarization is referred to the orientation of the electrical field of the electromagnetic wave.

A single polarized SAR system is a SAR system which transmits one horizontally or vertically polarized signal and receives the horizontal or vertical polarized component of the returned

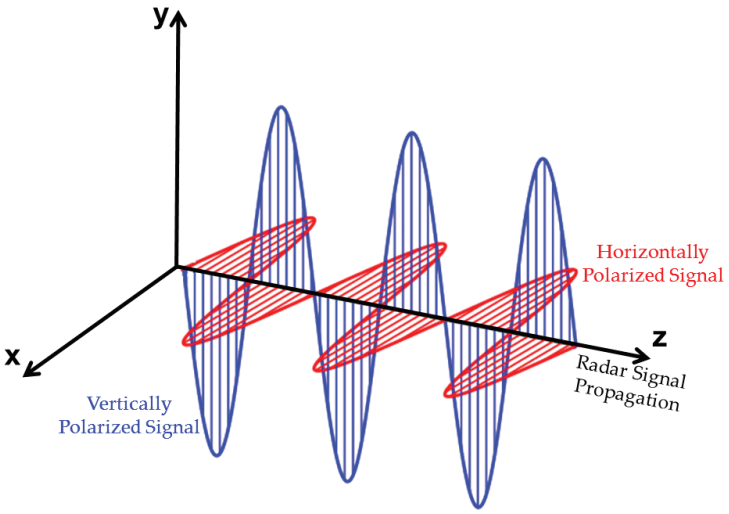

Figure 3. Horizontally and vertically polarized radar signal.

signal. A dual polarized SAR system is a SAR system which transmits one horizontally or vertically polarized signal and receives both the horizontal and vertical polarized components of the returned signal. A single or dual polarized SAR system acquires partial information with respect to the full polarimetric state of the radar target. A fully polarimetric SAR system transmits alternatively horizontally and vertically polarized signal and receives returns in both orthogonal polarizations, allowing for complete information of the radar target [6, 8]. While full polarimetric SAR systems provide complete information about the radar target, the coverage of these systems is half of the coverage of single or dual polarized SAR systems. Also, the energy required by the satellite for the acquisition of full polarimetric SAR imagery and the pulse repetition frequency of the SAR sensor are twice the single or dual polarized SAR systems.

A new SAR configuration named compact polarimetric SAR is currently being implemented in SAR systems, where a circular polarized signal (**Figure 4**) is transmitted and two orthogonal polarizations (horizontal and vertical) are coherently received [9]. Thus, the relative phase between the two receiving channels is preserved and calibrated, but the swath coverage is not reduced.

In comparison to the full polarimetric SAR systems, compact polarimetric SAR operates with half pulse repetition frequency, reducing the average transmit power and increasing the swath width. Consequently, this SAR configuration is associated with low-cost and low-mass constraints of the spaceborne polarimetric SAR systems. The wider coverage of the compact SAR system reduces the revisit time of the satellite, making this system operationally viable [10]. These advantages come with an associated cost in the loss of full polarimetric information. Hence, generally, a compact polarimetric SAR system cannot be "as good as" a full polarimetric system [11]. Such SAR architecture is already included in the current Indian Radar Imaging Satellite-1 (RISAT-1) and the Japanese Advanced Land Observing Satellite-2 (ALOS-2) carrying the Phased Array type L-band Synthetic Aperture Radar-2 (PALSAR-2). Also, compact polarimetric SAR will be included in the future Canadian RADARSAT Constellation Mission (RCM).

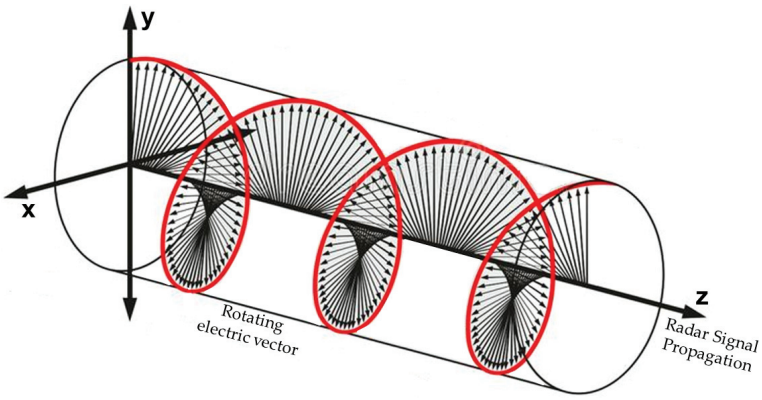

Figure 4. Circular polarized radar signal.

2.1. Polarimetric scattering vector

Fully polarimetric SAR systems measure the complete polarimetric information of a radar target in the form of a scattering matrix [S]. The scattering matrix [S] is an array of four complex elements that describes the transformation of the polarization of a wave pulse incident upon a reflective medium to the polarization of the backscattered wave and has the form [6]:

$$[S] = \begin{bmatrix} HH & HV \\ VH & VV \end{bmatrix} \tag{1}$$

where H and V refer to horizontal and vertical polarized signals, respectively. The elements of the scattering matrix [S] are complex scattering amplitudes. For most natural targets including wetlands, the reciprocity assumption holds where HV = VH. The diagonal elements HH and VV are called co-polarized elements, while the off-diagonal elements HV and VH are called cross-polarized elements. Two polarimetric scattering vectors can be extracted from the target scattering matrix, which are the lexicographical scattering vector and the Pauli scattering vector [12]. Assuming the reciprocity condition, the lexicological scattering vector has the form:

$$K_l = [HH\ VV\ 2HV]^T \tag{2}$$

where the superscript T denotes the vector transpose. The multiplication of the cross-polarization with 2 is to preserve the total backscattered power of the returned signal. The Pauli scattering vector can be obtained from the complex Pauli spin matrices [6] and, assuming the reciprocity condition, has the form:

$$K_p = \frac{1}{\sqrt{2}}[HH + VV\ HH - VV\ 2HV]^T \tag{3}$$

Deterministic scatterers can be described completely by a single scattering matrix or vector. However, for remote sensing SAR applications, the assumption of pure deterministic scatterers is not valid. Thus, scatterers are non-deterministic and cannot be described with a single polarimetric scattering matrix or vector. This is because the resolution cell is bigger than the wavelength of the incident wave. Non-deterministic scatterers are spatially distributed. Therefore, each resolution cell is assumed to contain many deterministic scatterers, where each of these scatterers can be described by a single scattering matrix [S_i]. Therefore, the measured scattering matrix [S] for one resolution cell consists of the coherent superposition of the individual scattering matrices [S_i] of all the deterministic scatterers located within the resolution cell [6, 12].

An ensemble average of the complex product between the lexicological scattering vector K_l and K_l^{*T} leads to the so-called polarimetric covariance matrix [C], which has the form [6]:

$$[C] = K_l.K_l^{*T} = \left\langle \begin{bmatrix} |HH|^2 & HHVV^* & \sqrt{2}HHHV^* \\ VVHH^* & |VV|^2 & \sqrt{2}VVHV^* \\ \sqrt{2}HVHH^* & \sqrt{2}HVVV^* & 2|HV|^2 \end{bmatrix} \right\rangle \tag{4}$$

where $\langle \ldots \rangle$ denotes a spatial ensemble averaging assuming homogeneity of the random scattering medium and * the complex conjugate. Analogously, the so-called polarimetric coherency matrix [T] is formed by the complex product of the Pauli scattering vector K_p with its complex conjugate transpose K_p^{*T} and takes the form [6]:

$$[T] = K_p.K_p^{*T} = \frac{1}{2}\left\langle \begin{bmatrix} |HH+VV|^2 & (HH+VV)(HH-VV)^* & 2(HH+VV)HV^* \\ (HH-VV)(HH+VV)^* & |HH-VV|^2 & 2(HH-VV)HV^* \\ 2HV(HH+VV)^* & 2HV(HH-VV)^* & 4|HV|^2 \end{bmatrix} \right\rangle \tag{5}$$

The relationship between the covariance matrix [C] and the coherency matrix [T] is linear. Both matrices are full rank, hermitian positive semidefinite and have the same real non-negative eigenvalues, but different eigenvectors. Moreover, both matrices contain the complete information about variance and correlation for all the complex elements of the scattering matrix [S] [12].

A compact polarimetric SAR system transmits a right- or left-circular polarized signal, providing a scattering vector of two elements:

$$K_c = [RH\ RV]^T \tag{6}$$

where R refers to a transmitted right-circular polarized signal. A four-element vector called Stokes vector [g] can be calculated from the measured compact polarimetric scattering vector, as follow [11]:

$$[g] = \begin{bmatrix} g_0 \\ g_1 \\ g_2 \\ g_3 \end{bmatrix} = \left\langle \begin{bmatrix} |RH|^2 + |RV|^2 \\ |RH|^2 - |RV|^2 \\ 2\mathrm{Re}(RHRV^*) \\ -2\mathrm{Im}(RHRV^*) \end{bmatrix} \right\rangle \tag{7}$$

where Re and Im are the real and imaginary parts of a complex number. The first Stokes element g_0 is associated with the total power of the backscattered signal while the fourth Stokes vector is associated with the power in the right-hand and left-hand circularly polarized component [13]. The elements of the Stokes vector can be used to derive an average coherency matrix, which takes the form [14]:

$$[T_c] = \frac{1}{2}\begin{bmatrix} g_0 + g_1 & g_2 + ig_3 \\ g_2 - ig_3 & g_0 - g_1 \end{bmatrix} \tag{8}$$

2.2. Polarimetric scattering mechanisms

Radar backscattering is a function of the radar target properties (dielectric properties, roughness, target geometry) and the radar system characteristics (polarization, band, incidence angle). Three major backscattering mechanisms can take place during the backscattering process. These are the surface, double bounce and volume scattering mechanism (**Figure 5**).

In the case of surface scattering mechanism (**Figure 5**), the incident radar signal features one or an odd number of bounces before returns back to the SAR antenna. In this case, a phase shift of 180° occurs between the transmitted and the received signal [6]. However, a very smooth surface could cause the radar incident signal to be reflected away from the radar antenna, causing the radar target to appear dark in the SAR image. In this case, scattering is called specular scattering. An example of such surfaces is the open water in wetlands [12]. In the case of double bounce scattering mechanism (**Figure 5**), the incident radar signal hits two surfaces, horizontal and adjacent vertical forming a dihedral angle, and almost all of incident waves return back to the radar antenna. Thus, the scattering from radar targets with double bounce scattering is very high. The phase difference between the transmitted and the received signal is equal to zero. Double bounce scattering mechanism is frequently observed in open wetlands, such as bog and marsh, as the results of the interaction of the radar signal between the standing water and vegetation [15]. In the case of volume scattering mechanism (**Figure 5**), the radar signal features multiple random scattering within the natural medium. Usually, a large portion of the transmitted signal is returned back to the SAR sensor, causing rise to cross polarizations (HV and VH). Thus, illuminated radar targets with volume scattering appear bright in a SAR image. Volume scattering is commonly observed in flooded vegetation wetlands due to multiple scattering in the vegetation canopy.

In general, the penetration capabilities and the attenuation depth of radar signal in a medium, such as flooded vegetation, increases with the increasing of the wavelength [6, 12]. **Figure 6** presents the penetration of radar signals for different bands. As shown in **Figure 6**, X-band SAR has a short wavelength signal with limited penetration capability, while L-band SAR has long wavelength signal with higher penetration capability. C-band SAR is assumed as a good compromise between X- and L-band SAR systems. As shown in **Figure 6**, the scattering mechanism of a radar target could be affected by the penetration depth of the radar signal. Thus, dense flooded vegetation could present volume scattering mechanism in X- or C-band SAR (return from canopy), but double bounce scattering mechanism in L-band due to scattering process from trunk-water interaction (**Figure 6**) [12].

Different decomposition methods have been proposed to derive the target scattering mechanisms for both full polarimetric [6, 16–24] and compact polarimetric [11, 25] SAR data. One of the earliest and widely used decomposition methods is the Cloude-Pottier decomposition [17].

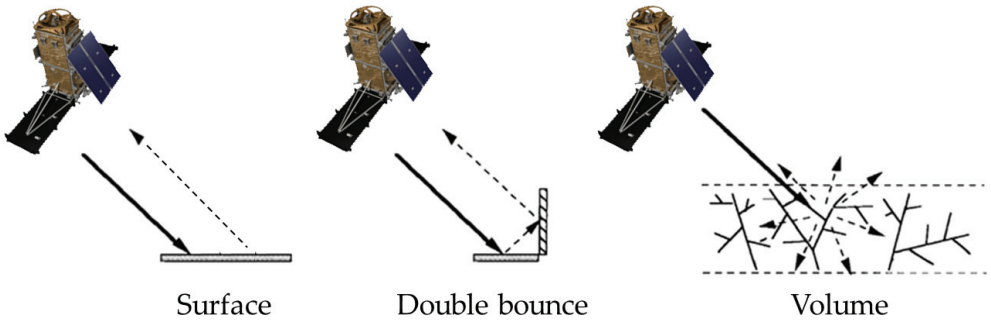

Figure 5. The three major scattering mechanisms: surface, double bounce and volume.

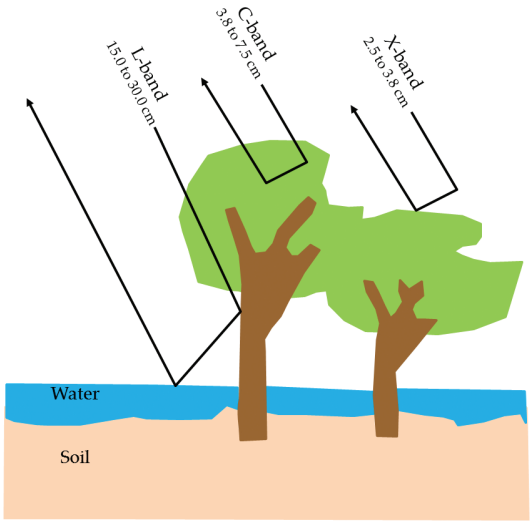

Figure 6. The radar signal penetration for different bands.

This method is incoherent decomposition method based on the eigenvector and eigenvalue analysis of the coherency matrix [T]. Given that [T] is hermitian positive semidefinite matrix, it can always be diagonalized using unitary similarity transformations. That is, the coherency matrix can be given as

$$[\mathrm{T}] = [\mathrm{U}][\Lambda][\mathrm{U}]^{*T} = [\mathrm{U}]\begin{bmatrix} \lambda_1 & 0 & 0 \\ 0 & \lambda_2 & 0 \\ 0 & 0 & \lambda_3 \end{bmatrix}[\mathrm{U}]^{*T} \tag{9}$$

where [Λ] is the diagonal eigenvalue matrix of [T], $\lambda_1 \geq \lambda_2 \geq \lambda_3 \geq 0$ are the real eigenvalues and [U] is a unitary matrix whose columns correspond to the orthogonal eigenvectors of [T]. Based on the Cloude-Pottier decomposition, three parameters can be derived [17]. The polarimetric entropy H ($0 \leq H \leq 1$) is defined by the logarithmic sum of the eigenvalues

$$\mathrm{H} = -\sum_{\mathrm{i}=1}^{3} \mathrm{P_i} \log_3 \mathrm{P_i} \tag{10}$$

where $\mathrm{P_i} = \lambda_\mathrm{i} / \sum_{\mathrm{i}=1}^{3} \lambda_\mathrm{i}$. This parameter is an indicator of the number of effective scattering mechanisms which took place in the scattering process [6]. The anisotropy A ($0 \leq A \leq 1$) describes the proportions between the secondary scattering mechanisms

$$\mathrm{A} = \frac{\lambda_2 - \lambda_3}{\lambda_2 + \lambda_3} \tag{11}$$

The anisotropy A provides additional information only for medium values of H because in this case secondary scattering mechanisms, in addition to the dominant scattering mechanism,

play an important role in the scattering process [6]. The alpha angle α ($0 \le \alpha \le 90^{o}$) provides information about the type of scattering mechanism

$$\alpha = \sum_{i=1}^{3} P_i \alpha_i \tag{12}$$

where $\cos(\alpha_i)$ in the magnitude of the first component of the coherency matrix eigenvector e_i ($i = 1, 2, 3$).

Another widely used polarimetric decomposition method is the Freeman-Durden method [18]. Contrary to the Cloude-Pottier decomposition, which is a purely mathematical construct, the Freeman-Durden decomposition method is a physically model-based incoherent decomposition based on the polarimetric covariance matrix. It relies on the conversion of a covariance matrix to a three-component model. The results of this decomposition are three coefficients corresponding to the weights of different model components. A polarimetric covariance matrix [C] can be decomposed to a sum of three components, corresponding to volume, surface, and double bounce scattering mechanisms [18]:

$$[C] = f_v[C]_v + f_s[C]_s + f_d[C]_d \tag{13}$$

where f_v, f_s, and f_d are the three coefficients corresponding to volume, surface, and double bounce scattering, respectively. The Freeman-Durden decomposition is particularly well adapted to the study of vegetated areas [18]. Thus, it is widely used for multitemporal wetland monitoring to track changes of shallow open water to flooded vegetation [26].

Scattering mechanism information can also be obtained using compact polarimetric SAR data. Two decomposition methods are commonly used. The first is the m-δ decomposition method [11], which is based on the degree of polarization of the backscattered signal $m = \sqrt{g_1^2 + g_2^2 + g_3^2}/g_0$ and the relative phase $\delta = \operatorname{atan}(g_3/g_2)$ and has the form [11]:

$$\begin{bmatrix} V_d \\ V_v \\ V_s \end{bmatrix} = \begin{bmatrix} \sqrt{g_0 m \dfrac{(1 - \sin\delta)}{2}} \\ \sqrt{g_0(1-m)} \\ \sqrt{g_0 m \dfrac{(1 + \sin\delta)}{2}} \end{bmatrix} \tag{14}$$

where V_d, V_v, and V_s refer to double bounce, volume, and surface scattering mechanisms, respectively. The second decomposition method is the m-χ decomposition [25], which is based on the degree of polarization m and the ellipticity $\chi = \operatorname{asin}(-g_3/mg_0)/2$, and has the form [25]:

$$\begin{bmatrix} P_d \\ P_v \\ P_s \end{bmatrix} = \begin{bmatrix} \sqrt{g_0 m \dfrac{(1 + \sin 2\chi)}{2}} \\ \sqrt{g_0(1-m)} \\ \sqrt{g_0 m \dfrac{(1 - \sin 2\chi)}{2}} \end{bmatrix} \tag{15}$$

where P_d, P_v and P_s refer to even bounce, volume, and odd bounce scattering mechanisms, respectively.

3. SAR wetland applications

3.1. Change detection

The accurate, effective, and continuous identification and tracking of changes in wetlands is necessary for monitoring human, climatic and other effects on these ecosystems and better understanding of their response. Wetlands are expected to be even more dynamic in the future with rapid and frequent changes due to the human stresses on environment and the global warming [27]. Different methodologies can be adopted to detect and track changes in wetlands using SAR imagery, depending on the type of the change and the available polarization option. For example, a change in the surface water level of a wetland area due to e.g. heavy rainfall could extend the wetland water surface, causing flooding in the surrounding areas. Such a change can be easily detected using SAR amplitude images before and after the event acquired with similar acquisition geometry. The specular scattering of the radar signal can highlight the open water areas (dark areas due to low returned signal). Spatiotemporal changes in wetlands as dynamic ecosystems could be interpreted using SAR amplitude imagery only. This is because changes within wetlands could change the surface type illuminated by the radar. Sometimes, the change could be more complex with alternations in surface water, flooded vegetation and upland boundaries. In this case, the additional polarimetric information from full or compact polarimetric SAR is necessary for the detection and interpretation of changes within wetlands.

As shown in **Figure 7**, a change within a wetland from wet soil with a high dielectric constant to open water is usually accompanied with a change in the radar backscattering from surface scattering with a strong returned signal (**Figure 7a**) to specular reflection with a weak returned signal (**Figure 7b**). The change in wetland could also be due to its seasonal development over time. Hence, intermediate marsh with large vegetation stems properly oriented could allow for double bounce scattering mechanism (**Figure 7c**). As the marsh develops, the strong observed double bounce scattering mechanism gradually decreases in favor of the volume scattering (**Figure 7d**) from the dense canopy of the fully developed marsh [28]. Thus, polarimetric decomposition methods enable the identification of wetland classes (e.g. flooded vegetation) and monitoring changes within these classes by means of the temporal change in the backscattering mechanisms. The role of decomposition methods for identification and monitoring of wetlands was highlighted in a number of recent studies [26, 29–31]. Another way of monitoring changes within wetlands could be through polarimetric change detection methodologies using full [10], compact [10, 32], or even coherent dual [33] polarized SAR imagery. These methodologies are based on polarimetric coherency/covariance matrices. Herein, changes are flagged without information about the scattering mechanisms, which occurred during the scattering process. Test statistics, such as those proposed in [34, 35], were proven effective for polarimetric change detection over wetlands.

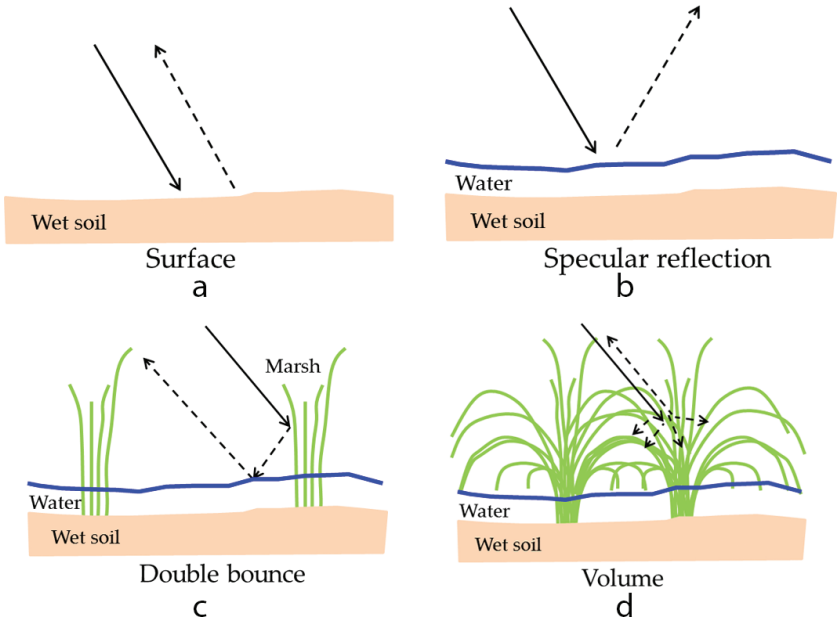

Figure 7. (a) Surface scattering mechanism from wet soil, (b) radar signal reflection from shallow open water, (c) double bounce scattering mechanism from signal interaction with vegetation stems and water surface and (d) volume scattering due to random scattering within the dense flooded vegetation canopy.

3.2. Wetland mapping

Ever since the launch of the Earth Resources Technology Satellite (ERTS) in 1972 there has been interest in using satellite remote sensing as a tool for wetland mapping and classification because the traditional air photo and field visit approaches are too costly and time consuming [36]. Wetlands are difficult to map and classify due to a large degree of spatial and temporal variability as well as structural and spectral similarities between wetland classes. Over the last decade or so a state-of-the-art approach for wetland classification has emerged. This is an object based classification approach using multi-source input data (optical and SAR) with a machine learning classification algorithm and a quality Digital Elevation Model (DEM) for identifying terrain suitability for wetlands or surface water [37–40]. Using this approach, greater than 90% accuracy is often achieved for a wide variety of wetland classification systems [41].

The early satellite SAR systems produced single channel intensity only output data, which limited its value for land cover and wetland classification. This type of data when used synergistically with optical data improved the wetland classification compared to using optical data alone but only to a minor degree [37, 42–45]. This is largely due to the ability of the SAR wavelengths to penetrate wetland vegetation and "see" the underlying water, thereby improving the flooded vegetation class discrimination. The flooded vegetation tends to produce a double bounce scattering mechanism, as explained earlier, which increases the intensity of the backscatter. HH polarization is best for this due to the enhanced penetration in vegetation.

As one goes up the polarization hierarchy from single channel intensity only data to dual-channel, compact polarimetry, and full polarimetry data sets the information content increases and the wetland classification subsequently improves [11, 46–50]. In general, dual channel SAR's and polarization ratios outperform single channel intensity only data systems and compact polarimetric data is better than dual channel data. Fully polarimetric data consistently shows the best information content for wetland classification by using polarimetric parameters derived from the data matrices, or polarimetric decompositions such as the Cloude and Pottier [17], Freeman-Durden [18], or Touzi [24] decompositions. You can use the decompositions or polarimetric parameters such as the polarization phase difference to identify flooded vegetation due to the double bounce effect increasing intensity and producing the phase shift. The Shannon Entropy has also proven useful for wetland mapping [51] and may have some benefit for finding the transition from flooded to saturated soil and between flooded vegetation and open water. This is a two-parameter model with one parameter relating to intensity and the other polarization diversity, and it may be simpler than using the decompositions.

There have been numerous frequency effect evaluations since the early observations of enhanced scattering from flooded vegetation on SEASAT imagery [52]. This effect for swamps and many vegetated wetlands with high biomass is quite evident in L-band data due to the increased canopy penetration and better interaction with the water/trunk/stem interface, resulting in the double bounce scattering mechanism [53, 54]. It is also evident at C-band and in some cases at X-band depending on the biomass and density of the canopy and the subsequent wavelength dependent penetration [41, 55–60]. In general, X- and C-band are preferred for herbaceous wetlands and less dense canopies while L-band is preferred for woody wetlands such as swamps and other wetland classes with high biomass.

SAR data has also proven effective for mapping peatlands, which is becoming more important because of climate change and carbon emission issues [61–64]. Due to the penetration of these longer wavelengths and the ability to penetrate beneath the plant canopy, there have been some indications that L-band polarimetric SAR can be used to differentiate between bog and fen peatlands due to the sensitivity of the water flow characteristics beneath the surface [65].

SAR does not penetrate water so provides little information on invasive aquatic submersive plants, but L-band and to a lesser degree C-band have shown some success at identifying invasive *Phragmites* [66]. This tall dense invasive provides significant SAR backscatter and can be separated from other land-cover due to this characteristic and its location in the landscape. It helps to use LiDAR as well as SAR due to the relative height and landscape position of the *Phragmites* [67].

In general, one wants to use a steep incidence angle for woody wetlands or flooded vegetation mapping in order to enhance the penetration to reach the water surface and realize the enhanced scattering effect due to double bounce scattering between the vegetation and the water surface. A shallow angle may be preferred if the focus is on the open water mapping as this can enhance the contrast between the specular scattering of surface water and the flooded vegetation with volume and double bounce scattering. Recent reviews of wetland remote sensing and SAR are provided in [40, 41, 68–70].

3.3. Dynamic surface water and flooded vegetation mapping

The specular backscatter from calm water surfaces allows for easy discrimination of open water from upland and flooded vegetation using SAR data. At the same time, the double bounce scattering from flooded vegetation allows discrimination from upland and open water as described earlier. This, combined with the all-weather data collection capabilities, makes SAR an ideal sensor for mapping flood as well as dynamic surface water and flooded vegetation [40].

Flood mapping is operational with SAR data in many countries using data from a variety of SAR systems from X- to L-band (see for example [71–74]). Intensity thresholding techniques have traditionally been used for open water mapping [75]. Texture, cross-polarization data, and other techniques are being developed to solve the problem when the water is brighter due to wind or current induced roughness, as well as to automate the process [76–79].

As described in the section on wetland mapping the double bounce effect and enhanced scattering from flooded vegetation makes SAR a good sensor for mapping flooded vegetation from non-flooded vegetation [40, 59, 80]. This allows the delineation of wetland extent and with multi-temporal data can be very useful for monitoring seasonal and/or annual changes in the wetland size and extent. [81] showed that flooded vegetation tends to remain coherent using InSAR techniques and this can then be used to map wetland type and extent. Thus, SAR is an ideal sensor for monitoring the spatially and temporally dynamic flooded vegetation components of wetlands.

The development of standard coverages, like that used for the Sentinel program, results in stacks of data with the same geometry and facilitates the use of temporal filters for speckle noise reduction. The use of a multi-temporal filter rather than the conventional spatial filtering approach can be an effective way to reduce the speckle while maintaining the spatial resolution and the ability to detect small objects and edges [82, 83]. This also allows the use of intensity metrics rather than thresholds to separate water from land, which can also help solving the wind roughness problem [84]. The multi-temporal coverage provided by SAR systems enables generating hydro-period and dynamic surface water as well as flooded vegetation masks [85, 86]. This enables better mapping of temporary, seasonal and ephemeral water bodies as well as the permanent water bodies, which are static and much easier to map. A recent review of SAR flood mapping and flood studies with SAR is provided in [87], while [88] provides a review of flooded vegetation mapping with SAR.

3.4. Water level monitoring

Wetland interferometric synthetic aperture radar (InSAR) is a relatively new application of the InSAR technology that detects water level changes over wide areas with 5–100 m pixel resolution and several centimeters vertical accuracy [89–91]. The wetland InSAR technique works where vegetation emerges above the water surface due to the “double bounce” effect, in which the radar pulse is backscattered twice from the water surface and vegetation [53]. InSAR observations were successfully used to study wetland hydrology in the Everglades [90–93], Louisiana [94–96] and the Sian Ka’an in Yucatan [97].

One of the key issues in using the InSAR observations for assessing wetland hydrology is the calibration of the InSAR observations, which are relative in both space and time. In time, the measurements provide the change in water level (not the actual water level) that occurred between the two data acquisitions. In space, the measurements describe the relative change of water levels in the entire interferogram with respect to a zero change at an arbitrary reference point, because the actual range between the satellite and the surface cannot be determined accurately. However, the relative changes between pixels can be determined at the cm-level. In many other InSAR applications, such as earthquake or volcanic induced deformation, the reference zero change point is chosen to be in the far-field, where changes are known to be negligible [98]. However, in wetland InSAR, the assumption of zero surface change in the far-field does not hold, because flow and water levels can be discontinuous across the various water control structures or other flow obstacles.

The calibration stage requires additional information on water level changes, which can be derived from various sources. In areas monitored by stage (water level) stations, as in the Everglades, the stage data can be used for the InSAR calibration, as conducted by [90]. Another calibration technique relies on spaceborne radar altimetry, which detects absolute water level changes over a few km wide footprints with accuracy of 5–10 cm [94]. However, the altimetry observations are limited in space and time, as the radar altimeter data can only be acquired along the satellite tracks, which are spaces roughly 100 km apart. Also, the altimetry data is not always synchronized with the InSAR observations, which are acquired by different satellites.

3.5. Wetland biomass estimation

Wetland biomass is of increasing interest due to methane emission contributions to climate change from degraded and thawing wetlands. Wetland change can also be used as an indicator of climate change impacts. Wetland vegetation biomass can therefore be an important indicator of carbon sequestration in wetlands and is essential for understanding the carbon cycle of these ecosystems. SAR data has the potential to estimate vegetation biomass in wetlands because radar is particularly sensitive to the vegetation canopy over an underlying water surface [99]. The biomass of totora reeds and bofedal in water-saturated Andean grasslands was mapped with ERS-1 data in [100]. The goal was to protect this ecosystem from overgrazing. They found that the backscatter signal of ERS-1 was sensitive to the humid and dry biomass of reeds and grasslands and their biomass maps were useful for the livestock management in the study region. [101] developed regression and analytical models for estimating mangrove wetland biomass in South China using RADARSAT images. [102, 103] also found that L-band ALOS PALSAR can be used to estimate the aboveground biomass because of the correlation between HH and HV backscatter signals. C-band backscatter characteristics from RADARSAT-2 data were used by [104] to estimate the biomass of the Poyang Lake wetlands in China. Also, [105] used ENVISAT ASAR data to estimate wetland vegetation biomass in Poyang Lake. These studies have shown that it is possible to estimate above water biomass in wetlands with SAR data.

4. Trends in wetland mapping and monitoring with SAR

As shown in the previous section, spaceborne SAR remote sensing technology is recognized as essential tool for effective wetland observation. With the presence of global warming and its associated risks on Earth systems, there is an expressed interest in increased temporal and spatial resolution of satellite measurements. Thus, a trend toward increased temporal and spatial resolution of SAR imagery is noted in recent and future SAR missions. The Sentinel-1 SAR mission with its two identical SAR satellites (Sentinel-1A&B) is a good example of a recent SAR mission with a spatial resolution ranging from 5 m to 100 m and a revisit time of 6 days. This high temporal and spatial resolution is expected to be even higher in the near future with the launch of the RCM in late 2018. The RCM is expected to provide SAR imagery in a spatial resolution ranging from 1 m to 100 m, in a revisit time of only 4 days [32]. The increased temporal and spatial resolution would be required to adequately monitor wetlands and characterize the actual implications of climate change. Also, it is expected to further improve our understanding of climate change in wetlands and water quality, allowing ecosystem managers and decision makers to have sufficient information regarding wetland preservation.

With the availability of different remote sensing data with various information contents, the application of multi-source data for advanced wetland applications is demonstrated in a number of studies; see for example [2, 44, 61, 67, 106]. In addition to SAR imagery, experiments on the integration of topographic and remote sensing data, such as optical imagery and LiDAR data, were conducted. The ultimate objective of these experiments was the improved mapping accuracy of wetlands. The integration of SAR imagery with optical and topographic data from multiple sensors was shown in [44, 106] to be necessary for improved wetland mapping and classification during the growing season. However, the integration of SAR imagery and LiDAR data did not improve significantly the classification accuracy of wetland in [61, 67]. The modern advances in remote sensing technology and the availability of multi-source information are shifting the manner in which Earth observation data are used for wetland monitoring, indicating the need for automated and efficient techniques. Different studies, such as [2, 44, 61, 106], have highlighted the effectiveness of machine learning algorithms for automated wetland classification. An example of these algorithms is the Random Forest (RF) classification algorithm proposed in [107]. This shift toward the automated machine learning algorithms comes to fulfill the requirement for operational wetland monitoring systems.

The continuing advancements in computer processing power and software development as well as the trend toward free and open access to remote sensing imagery, such as those from the current Sentinel satellites and the future RCM, are enabling the ingestion of data into a centralized archive. This also supports the application of a standard rapid processing chain to generate analysis-ready wetland products. The provision of analysis-ready products to a wide range of users would revolutionize the role of remote sensing in Earth system science [108].

5. Conclusions

This chapter highlighted the SAR remote sensing technology and its potential for wetland monitoring and mapping. It was shown that a wide range of wetland applications can be

addressed using SAR remote sensing imagery. SAR data with enhanced target information provided by full or compact polarimetric SAR systems can provide information for advanced wetland applications. In many studies, the information about the polarimetric scattering mechanisms was found necessary for observing the temporal development of wetlands and detecting their changes. This chapter shows that the fusion of multi-source data improves wetland mapping, especially during the growing season. Furthermore, a relatively new application of the InSAR technology is currently implemented for water level monitoring. Given the problem of climate change, wetland biomass estimation using SAR imagery is becoming necessary for the evaluation of methane emission contributions to climate change from degraded and thawing wetlands. The current advanced computing capabilities along with the shift toward free and open access remote sensing data are enabling analysis-ready products for a wide range of users.

Acknowledgements

Authors would like to thank Mr. Jean Granger and Dr. Bahram Salehi from the Memorial University of Newfoundland and Dr. Koreen Millard form Environment and Climate Change Canada for their help in providing pictures of different wetland classes.

Conflict of interest

Authors declare no conflict of interest.

Acronyms and abbreviations

SAR	synthetic aperture radar
HH	horizontal transmitted horizontal received signal
VV	vertical transmitted vertical received signal
HV	horizontal transmitted vertical received signal
VH	vertical transmitted horizontal received signal
RH	right circular transmitted horizontal received signal
RV	right circular transmitted vertical received signal
RISAT-1	Radar Imaging Satellite-1
ALOS-2	Advanced Land Observing Satellite-2
PALSAR-2	Phased Array type L-band Synthetic Aperture Radar-2
RCM	RADARSAT Constellation Mission

InSAR	interferometric synthetic aperture radar
RF	random forest
DEM	digital elevation model

Author details

Mohammed Dabboor[1]* and Brian Brisco[2]

*Address all correspondence to: mohammed.dabboor@canada.ca

1 Science and Technology Branch, Environment and Climate Change Canada, Government of Canada, Dorval, Quebec, Canada

2 Canada Center for Mapping and Earth Observation, Natural Resources Canada, Government of Canada, Ottawa, Ontario, Canada

References

[1] National Wetlands Working Group. In: Warner B, Rubec C, editors. The Canadian Wetland Classification System. Waterloo, Ontario: Wetlands Research Centre, University of Waterloo; 1997

[2] Jahncke R, Leblon B, Bush P, LaRocque A. Mapping wetlands in Nova Scotia with multibeam RADARSAT-2 Polarimetric SAR, optical satellite imagery, and Lidar data. International Journal of Applied Earth Observation and Geoinformation. 2018;**68**:139-156

[3] Mitsch WJ, Gosselink JG. Wetlands. Hoboken, New Jersey, USA: John Wiley & Sons; 2007

[4] Zoltai SC, Vitt DH. Canadian wetlands: Environmental gradients and classification. Vegetatio. 1995;**118**(1):131-137

[5] Martin J. Mapping Wetland Areas on Forested Landscapes using Radarsat-2 and Landsat-5 TM Data. Master's Thesis, University of New Brunswick, Fredericton, NB, Canada, Saint John, NB, Canada, 2012

[6] Lee JS, Pottier E. Polarimetric Radar Imaging: From Basics to Applications. Boca Raton, FL, USA: CRC Press; 2009

[7] Catry T, Li Z, Roux E, Herbreteau V, Gurge H, Mangeas M, et al. Wetlands and malaria in the Amazon: Guidelines for the use of synthetic aperture radar remote-sensing. International Journal of Environmental Research and Public Health. 2018;**15**(3):1-27

[8] Ainswoith TL, Preiss M, Stacy N, Nord N, Lee JS. Analysis of compact Polarimetric SAR imaging modes. In: PolInSAR Workshop, Frascati, Italy. 2007

[9] Raney RK. Hybrid-Polarity SAR Architecture. IEEE Transactions on Geoscience and Remote Sensing. 2007;**45**(11):3397-3404

[10] Dabboor M, White L, Brisco B, Charbonneau F. Change detection with compact polarimetric SAR for monitoring wetlands. Canadian Journal of Remote Sensing. 2015;**41**(5): 408-417

[11] Charbonneau F, Brian B, Raney K, McNairn H, Liu C, Vachon P, et al. Compact polarimetry overview and applications assessment. Canadian Journal of Remote Sensing. 2010; **36**(2):S298-S315

[12] Dabboor M. New Segmentation Algorithms for Dual and Full. Polarimetric SAR Data. Calgary, AB: University of Calgary; 2010

[13] Dabboor M, Montpetit B, Howell S. Assessment of the high resolution SAR mode of the RADARSAT constellation mission for first year ice and multiyear ice characterization. Remote Sensing. 2018;**10**:594

[14] Cloude SR, Goodenough DG, Chen H. Compact decomposition theory. IEEE Geoscience and Remote Sensing Letters. 2012;**9**(1):28-32

[15] Li J, Chen W, Touzi R. Optimum RADARSAT-1 configurations for wetlands discrimination: A case study of the Mer Bleue peat bog. Canadian Journal of Remote Sensing. 2014; **33**(1):S46-S55

[16] Cloude SR, Pottier E. A review of target decomposition theorems in radar polarimetry. IEEE Transactions on Geoscience and Remote Sensing. 1996;**34**(2):498-518

[17] Cloude SR, Pottier E. An entropy based classification scheme for land applications of polarimetric SAR. IEEE Transactions on Geoscience and Remote Sensing. 1998;**35**(1):68-78

[18] Freeman A, Durden S. A three-component scattering model for polarimetric SAR data. IEEE Transactions on Geoscience and Remote Sensing. 1998;**36**(3):963-973

[19] Yamaguchi Y, Moriyama T, Ishido M, Yamad H. Four-component scattering model for polarimetric SAR image decomposition. IEEE Transactions on Geoscience and Remote Sensing. 2005;**43**(8):1699-1706

[20] Yamaguchi Y, Sato A, Boerner WM, Sato R, Yamada H. Four-component scattering power decomposition with rotation of coherency matrix. IEEE Transactions on Geoscience and Remote Sensing. 2011;**49**(6):2251-2258

[21] Sato A, Yamaguchi Y, Singh G, Park S-E. Four-component scattering power decomposition with extended volume scattering model. IEEE Geoscience and Remote Sensing Letters. 2012;**9**(2):166-170

[22] Singh G, Yamaguchi Y, Park SE. General four-component scattering power decomposition with unitary transformation of coherency matrix. IEEE Transactions on Geoscience and Remote Sensing. 2013;**51**(5):3014-3022

[23] Cui Y, Yamaguchi Y, Yang J, Kobayashi H, Park SE, Singh G. On complete model-based decomposition of polarimetric SAR coherency matrix data. IEEE Transactions on Geoscience and Remote Sensing. 2014;**52**(4):1991-2001

[24] Touzi R. Target scattering decomposition in terms of roll-invariant target parameters. IEEE Transactions on Geoscience and Remote Sensing. 2007;**45**(1):73-84

[25] Raney RK, Cahill JTS, Patterson GW, Bussey DB. The m-chi decomposition of hybrid dual-polarimetric radar data with application to lunar craters. Journal of Geophysical Research. 2012;**117**:E00H21

[26] White L, Brisco B, Dabboor M, Schmitt A, Pratt A. A collection of SAR methodologies for monitoring wetlands. Remote Sensing. 2015;**7**:7615-7645

[27] Ballanti L, Byrd KB, Woo I, Ellings C. Remote sensing for wetland mapping and historical change detection at the Nisqually river delta. Sustainability. 2017;**9**:1919

[28] Kwoun O-I, Lu Z. Multi-temporal RADARSAT-1 and ERS backscattering signatures of coastal wetlands in southeastern Louisiana. Photogrammetric Engineering & Remote Sensing. 2009;**11**(5):607-617

[29] Schmitt A, Brisco B. Wetland monitoring using the curvelet-based change detection method on polarimetric SAR imagery. Water. 2013;**5**:1036-1051

[30] Brisco B, Schmitt A, Murnaghan K, Kaya S, Roth A. SAR polarimetric change detection for flooded vegetation. International Journal of Digital Earth. 2011;**6**(2):1-12

[31] Gallant AL, Kaya SG, White L, Brisco B, Roth MF, Sadinski W, et al. Detecting emergence, growth, and senescence of wetland vegetation with polarimetric synthetic aperture radar (SAR) data. Water. 2014;**6**:694-722

[32] Dabboor M, Iris S, Singhroy V. The RADARSAT constellation mission in support of environmental applications. In: Proceedings; 2018

[33] Muro J, Canty M, Conradsen K, Hüttich C, Nielsen AA, Skriver H, et al. Short-term change detection in wetlands using Sentinel-1 time series. Remote Sensing. 2016;**8**:795

[34] Conradsen K, Nielsen AA, Skriver H. Determining the points of change in time series of polarimetric SAR data. IEEE Transactions on Geoscience and Remote Sensing. 2016; **54**(5):3007-3024

[35] Dabboor M, Collins M, Karathanassi V, Braun A. An unsupervised classification approach for polarimetric SAR data based on the Chernoff distance for complex Wishart distribution. IEEE Transactions on Geoscience and Remote Sensing. 2013;**51**(7):4200-4213

[36] Ozesmi SL, Bauer ME. Satellite remote sensing of wetlands. Wetlands Ecology and Management. 2002;**10**(5):381-402

[37] Grenier M, Demers AM, Labrecque S, Benoit M, Fournier RA, Drolet B. An object-based method to map wetlands using RADARSAT-1 and Landsat ETM images: Test case on two sites in Quebec, Canada. Canadian Journal of Remote Sensing. 2007;**33**(1):S28-S45

[38] Li J, Chen W. A rule-based method for mapping Canada's wetlands using optical, radar and DEM data. International Journal of Remote Sesning. 2011;**26**(22):5051-5069

[39] Knight JF, Corcoran J, Rampi L, Pelletier K. Theory and applications of object-based image analysis and emerging methods in wetland mapping. In: Tine RW, Lang MW, Klemas VV, editors. Remote Sensing of Wetlands: Applications and Advances. Boca Raton, Florida, USA: CRC Press; 2015

[40] Brisco B. Mapping and monitoring surface water and wetlands with synthetic aperture radar. In: Tine RW, Lang MW, Klemas VV, editors. Remote Sensing of Wetlands: Applications and Advances. Boca Raton, Florida, USA: CRC Press; 2015

[41] Mahdavi S, Salehi B, Granger J, Amani M, Brisco B, Huang W. Remote sensing for wetland classification: A comprehensive review. Journal GIScience and Remote Sensing. 2018;**55**(5):623-658

[42] Wang J, Shang J, Brisco B, Brown RR. Evaluation of multi-date ERS-1 and multispectral Landsat imagery for wetland detection in southern Ontario. Canadian Journal of Remote Sensing. 1998;**24**(1):60-68

[43] Toyra J, Pietroniro A, Martz LL. Multi-sensor hydrologic assessment of freshwater wetland. Remote Sensing of Environment. 2001;**75**(2):162-173

[44] Corcoran J, Knight J, Brisco B, Kaya S, Cull A, Murnaghan K. The integration of optical, topographic, and radar data for wetland mapping in northern Minnesota. Canadian Journal of Remote Sensing. 2011;**37**(5):564-582

[45] Koch M, Schmid T, Reyes M, Gumuzzio J. Evaluating full polarimetric C- and L-band data for mapping wetland conditions in a semi-arid environment in central Spain. IEEE Journal of Selected Topics in Applied Earth Observations and Remote Sensing. 2012;**5**(3): 1033-1044

[46] Baghdadi N, Bernier M, Gauthier R, Neeso I. Evaluation of C-band SAR data for wetlands mapping. International Journal of Remote Sensing. 2001;**22**(1):71-88

[47] Touzi R, Deschamps A, Rother G. Wetland characterization using polarimetric RADARSAT-2 capability. Canadian Journal of Remote Sensing. 2007;**33**(1):S56-SS67

[48] Brisco B, Kapfer M, Hirose T, Tedford B, Liu J. Evaluation of C-band polarization diversity and polarimetry for wetland mapping. Canadian Journal of Remote Sensing. 2011; **37**(1):82-92

[49] Brisco B, Kun L, Tedford B, Charbonneau F, Shao Y. Compact polarimetry assessment for rice and wetland mapping. International Journal of Remote Sensing. 2013;**34**(6):1949-1964

[50] Mleczko M, Mróz M. Wetland mapping using SAR data from the Sentinel-1A and Tan DEM-X missions: A comparative study in the Biebrza floodplain (Poland). Remote Sensing. 2018;**10**:78

[51] Marechal C, Pottier E, Hubert-Moy L, Rapinel S. One year wetland survey investigations from quad-pol RADARSAT-2 time-series SAR images. Canadian Journal of Remote Sensing. 2012;**38**(3):240-252

[52] Mac Donald HC, Waite WP, Demarcke JS. Use of Seasat satellite radar imagery. In: The American Society of Photogrammetry Annual Technical Meeting, Niagara Falls, New York. 1980

[53] Richards JA, Woodgate PW, Skidmor AK. An explanation of enhanced radar backscattering from flooded forests. International Journal of Remote Sensing. 1987;**8**(7):1093-1100

[54] Chapman B, McDonald K, Shimada M, Rosenqvist A, Schroeder R, Hess L. Mapping regional inundation with space-borne L-band SAR. Remote Sensing. 2015;**7**:5440-5470

[55] Pope KO, Rejmankova E, Paris JF, Woodruff R. Detecting seasonal flooding cycles in marches of the Yucatan Peninsula with SIR-C polarimetric radar imagery. Remote Sensing of Environment. 1997;**59**(2):157-166

[56] Costa MDF, de Moraes Novo E, Ahern F, Mitsuo F II, Mantovani JE, Ballester MV, et al. The Amazon floodplain through radar eyes: Lago Grande de Monte Alegre case study. Canadian Journal of Remote Sensing. 2014;**24**(4):339-349

[57] Novo EMLM, Costa MPF, Mantovani JE, Lima IBT. Relationship between macrophyte stand variables and radar backscatter at L and C band, Tucuruí reservoir, Brazil. International Journal of Remote Sensing. 2010;**23**(7):1241-1260

[58] Kasischke ES, Smith KB, Bourgeau-Chavez LL, Romanowicz EA, Brunzell S, Richardson CJ. Effects of seasonal hydrologic patterns in South Florida wetlands on radar backscatter measured from ERS-2 SAR imagery. Remote Sensing of Enviroment. 2003; **88**(4):423-441

[59] Plank S, Jüssi M, Martinis S, Twele A. Mapping of flooded vegetation by means of polarimetric Sentinel-1 and ALOS-2/PALSAR-2 imagery. International Journal of Remote Sensing. 2017;**38**(18):3831-3850

[60] Mahdianpari M, Salehi B, Mohammadimanesh F, Motagh M. Random forest wetland classification using ALOS-2 L-band, RADARSAT-2 C-band, and Terra SAR-X imagery. ISPRS Journal of Photogrammetry and Remote Sensing. 2017;**130**:13-31

[61] Millard K, Richardson M. Wetland mapping with LiDAR derivatives, SAR polarimetric decompositions, and LiDAR-SAR fusion using a RF classifier. Canadian Journal of Remote Sensing. 2014;**39**(4):290-307

[62] Reschke J, Bartsch A, Schlaffer S, Schepasch S, Schepaschenko D. Capability of C-band SAR for operational wetland monitoring at high latitudes. Remote Sensing. 2012;**4**(10): 2923-2943

[63] Lönnqvist A, Rauste Y, Molinier M, Häme T. Polarimetric SAR data in land cover mapping in boreal zone. IEEE Transactions on Geoscience and Remote Sensing. 2010; **48**(10):3652-3662

[64] Bourgeau-Chavez LL, Riordan K, Powell RP, Miller N, Nowels M. Improving wetland characterization with multi-Sensor, multi-temporal SAR and optical/infrared data fusion. In: Jedlovec G, editor. Advances in Geoscience and Remote Sensing. Rijeka: Intech Open; 2009

[65] Touzi R, Gosselin G, Brook R. Polarimetric L-band SAR for peatland mapping and monitoring. In: ESA Book on Principles and Applications of Pol-InSAR. Springer; 2015

[66] Bourgeau-Chavez L, Kowalski KP, Carlson Mazur ML, Scarbrough KA, Powell RB, Brooks CN, et al. Mapping invasive *Phragmites australis* in the coastal Great Lakes with ALOS PALSAR satellite imagery for decision support. Journal of Great Lakes Research. 2013;**39**(1):65-77

[67] Allen TR, Wang Y, Gore B. Coastal wetland mapping combining multi-date SAR and LiDAR. Geocarto International. 2013;**28**(7):616-631

[68] Henderson FM, Lewis AJ. Radar detection of wetland ecosystems: A review. International Journal of Remote Sensing. 2008;**29**(20):5809-5835

[69] Guo M, Li J, Sheng C, Xu J, Wu L. A review of wetland remote sensing. Sensors. 2017; **17**(4):777

[70] Wohlfart C, Winkler K, Wendleder A, Roth A. Terra SAR-X and wetlands: A review. Remote Sensing. 2018;**10**(6):916

[71] Alexakis DD, Hadjimitsis DG, Agapiou A, Themistocleous K, Retalis A, Michaelides S, et al. Flood mapping of Yialias River catchment area in Cyprus using ALOS PALSAR radar images. In: SPIE Remote Sensing for Agriculture, Ecosystems, and Hydrology XIV, Edinburgh, United Kingdom. 2012

[72] Refice A, Capolongo D, Pasquariello G, D'Addabbo A, Bovenga F, Nutricato R, et al. SAR and InSAR for flood monitoring: Examples with COSMO-Sky Med data. IEEE Journal of Selected Topics in Applied Earth Observations and Remote Sensing. 2014;**7**(7):2711-2722

[73] Adam S, Wiebe J, Collins M, Pietroniro A. Radarsat flood mapping in the Peace-Athabasca Delta, Canada. Canadian Journal of Remote Sensing. 2014;**24**(1):69-79

[74] Twele A, Cao W, Plank S, Martinis S. Sentinel-1-based flood mapping: A fully automated processing chain. International Journal of Remote Sensing. 2016;**37**(13):2990-3004

[75] Brisco B, Short N, van der Sanden JJ, Landry R, Raymond D. A semi-automated tool for surface water mapping with RADARSAT-1. Canadian Journal of Remote Sensing; 2009; **35**(4):336-344

[76] White L, Brisco B, Pregitzer M, Tedford B, Boychuck L. RADARSAT-2 beam mode selection for surface water and flood mapping. Canadian Journal of Remote Sensing. 2013;**40**(2):135-151

[77] Li J, Wang S. An automatic method for mapping inland surface waterbodies with Radarsat-2 imagery. International Journal of Remote Sensing. 2015;**36**(5):1367-1384

[78] Bolanos S, Stiff D, Brisco B, Pietroniro A. Operational surface water detection and monitoring using radarsat. Remote Sensing. 2016;**8**:285

[79] Behnamian A, Banks S, White L, Brisco B, Millard K, Pasher J, et al. Semi-automated surface water detection with synthetic aperture radar data. Remote Sensing. 2017;**9**:1209

[80] Horrit MS, Mason DC, Cobby DM, Davenport IJ, Bates PD. Waterline mapping in flooded vegetation from airborne SAR imagery. Remote Sensing of Environment. 2003; **85**(3):271-281

[81] Brisco B, Ahern F, Murnaghan K, White L, Canisus F, Lancaster P. Seasonal change in wetland coherence as an aid to wetland monitoring. Remote Sensing. 2017;**9**(2):158

[82] Quegan S, Yu JJ. Filtering of multichannel SAR images. IEEE Transactions on Geoscience and Remote Sensing. 2001;**39**(11):2373-2379

[83] Wegmuller U, Santoro M, Werner C. Multi-temporal SAR data filtering for land applications. In: ESA Living Planet Symposium, Edinburgh, UK. September 2013. pp. 9-13

[84] Santoro M, Wugmüller U. Multi-temporal synthetic aperture radar metrics applied to map open water bodies. IEEE Journal of Selected Topics in Applied Earth Observations and Remote Sensing. 2014;**7**(8):3225-3238

[85] DeLancey ER, Kariyeva J, Cranston J, Cranston J, Brisco B. Monitoring hydro temporal variability in Alberta, Canada with multi-temporal Sentinel-1 SAR data. Canadian Journal of Remote Sensing. 2018;**44**(1):1-10

[86] Montgomery J, Hopkinson C, Brisco B, Patterson S. Prairie Pothole Region wetland hydro-period classification using multi-temporal SAR in Alberta, Canada. Hydrological Processes. 2018;**32**(10):1-15

[87] Martinis S, Künzer C, Twele A. Flood studies using synthetic aperture radar data. In: Thenkabail P, editor. Remote Sensing Handbook Volume III-Remote Sensing of Water Resources, Disasters, and Urban Studies. Boca Raton, Florida, USA: CRC Press; 2015. pp. 145-173

[88] Tsyganskaya V, Martinis S, Marzahn P, Ludwig R. SAR-based detection of flooded vegetation – a review of characteristics and approaches. International Journal of Remote Sensing. CRC Press; 2018;**39**(8):2255-2293

[89] Alsdorf D, Smith L, Melack J. Amazon floodplain water level changes measured with interferometric SIR-C Radar. IEEE Transactions on Geoscience and Remote Sensing. 2001;**39**(2):423-431

[90] Wdowinski S, Amelung F, Miralles-Wilhelm F, Dixon TH, Carande R. Space-based measurements of sheet-flow characteristics in the Everglades wetland, Florida Space-based measurements of sheet-flow characteristics in the Everglades wetland, Florida. Geophysical Research Letters. 2004;**31**:L15503

[91] Wdowinski S, Kim SW, Amelung F, Dixon TH, Miralles-Wilhelm F, Sonenshein R. Space-based detection of wetlands' surface water level changes from L-band SAR interferometry. Remote Sensing of Environment. 2008;**112**(3):681-696

[92] Hong S-H, Wdowinski S, Kim S-W. Evaluation of Terra SAR-X observations for wetland InSAR application. IEEE Transactions on Geoscience and Remote Sensing. 2010;**48**(2): 864-873

[93] Hong SH, Wdowinski S, Kim SW, Won JS. Multi-temporal monitoring of wetland water levels in the Florida Everglades using interferometric synthetic aperture radar (InSAR). Remote Sensing of Environment. 2010;**114**(11):2436-2447

[94] Kim J-W, Lu Z, Lee H, Shum CK, Swarzenski CM, Doyle TW, et al. Integrated analysis of PALSAR/Radarsat-1 InSAR and ENVISAT altimeter. Remote Sensing of Environment. 2009;**113**(11):2356-2365

[95] Lu Z, Crane M, Kwoun O, Wells C, Swarzenski C, Rykhus R. C-band radar observes water level change in swamp forests. EOS Transactions, Americal Geophysical Union. 2005;**86**(14):141-144

[96] Lu Z, Kwoun OI. Radarsat-1 and ERS InSAR analysis over southeastern coastal Louisiana: Implications for mapping water-level changes beneath swamp forests. IEEE Transactions on Geoscience and Remote Sensing. 2008;**46**(8):2167-2184

[97] Gondwe BRN, Hong S-H, Wdowinski S, Bauer-Gottwein P. Hydrologic dynamics of the ground-water-dependent Sian Ka'an wetlands, Mexico, derived from InSAR and SAR data. Wetlands. 2010;**30**(1):1-13

[98] Massonnet D, Rossi M, Carmona C, Adragna F, Peltzer G, Feigl K, et al. The displacement field of the Landers earthquake mapped by radar interferometry. Nature. 1993; **364**:138-142

[99] Kasischke ES, Bourgeau-Chavez LL. Monitoring south Florida wetlands using ERS-1 SAR imagery. Photogrammetric Engineering and Remote Sensing. 1997;**63**(3):281-291

[100] Moreau S, Toan TL. Biomass quantification of Andean wetland forages using ERS satellite SAR data for optimizing livestock management. Remote Sensing of Environment. 2003;**84**(4):477-492

[101] Li X, Gar-On Yeh A, Wang S, Liu K, Liu X, Qian J, et al. Regression and analytical models for estimating mangrove wetland biomass in South China using Radarsat images. International Journal of Remote Sensing. 2007;**28**(24):5567-5582

[102] Hamdan O, Aziz HK, Hasmadi IM. L-band ALOS PALSAR for biomass estimation of Matang mangroves, Malaysia. Remote Sensing of Environment. 2014;**155**:69-78

[103] Darmawan S, Takeuchi W, Vetrita Y, Wikantika K, Sari DK. Impact of topography and tidal height on ALOS PALSAR polarimetric measurements to estimate aboveground biomass of mangrove forest in Indonesia. Journal of Sensors. 2015;**2015**:13. Article ID 641798

[104] Shen G, Liao J, Guo H, Liu J. Poyang Lake wetland vegetation biomass inversion using polarimetric RADARSAT-2 synthetic aperture radar data. 2015;**9**(1):451-455

[105] Liao J, Shen G, Dong L. Biomass estimation of wetland vegetation in Poyang Lake area using ENVISAT advanced synthetic aperture radar data. Journal of Applied Remote Sensing. 2013;**7**(1):073579

[106] Dubeau P, King DJ, Unbushe DG, Rebelo L-M. Mapping the dabus wetlands, Ethiopia, using random forest classification of Landsat, PALSAR and topographic data. Remote Sensing. 2017;**9**(10):1056

[107] Breiman L. Random forests. Machine Learning. 2001;**45**(1):5-32

[108] Bartuszevige A, Laurent E, Potter B. Integrating Remote Sensing Technology into Habitat Conservation Planning Tools: What Was Learned and Next Steps for Collaboration. U.S. NABCI Committee; 2015